Comparative analysis of formalisms and performances of three different beyond-mean-field approaches

F. Knapp,[1,*] P. Papakonstantinou,[2] P. Veselý,[3] G. De Gregorio,[4,5] J. Herko,[6] and N. Lo Iudice[7]

[1]*Institute of Particle and Nuclear Physics, Faculty of Mathematics and Physics, Charles University, V Holešovičkách 2, 180 00 Prague, Czech Republic*

[2]*Rare Isotope Science Project, Institute for Basic Science, Daejeon 34000, Korea*

[3]*Nuclear Physics Institute, Czech Academy of Sciences, 250 68 Řež, Czech Republic*

[4]*Dipartimento di Matematica e Fisica, Università degli Studi della Campania "Luigi Vanvitelli", viale Abramo Lincoln 5, I-81100 Caserta, Italy*

[5]*Istituto Nazionale di Fisica Nucleare, Complesso Universitario di Monte S. Angelo, Via Cintia, I-80126 Napoli, Italy*

[6]*Department of Physics and Astronomy, University of Notre Dame, Notre Dame, Indiana 46556-5670, USA*

[7]*Dipartimento di Fisica, Università di Napoli Federico II, 80126 Napoli, Italy*

(Received 6 November 2022; accepted 22 December 2022; published 12 January 2023)

We investigate the differences and analogies between the equation of motion phonon method (EMPM) and second Tamm-Dancoff and random-phase approximations (STDA and SRPA) paying special attention to the problem of spurious center-of-mass (c.m.) admixtures. In order to compare them on an equal footing, we perform self-consistent calculations of the multipole strength distributions in selected doubly magic nuclei within a space including up to two-particle–two-hole (2p-2h) basis states using the unitary correlation operator method two-body intrinsic Hamiltonian and we explore the tools each approach supplies for removing the spurious c.m. admixtures. We find that the EMPM and STDA yield exactly the same results when the same intrinsic Hamiltonian is used and the coupling of the Hartree-Fock state with the 2p-2h space is neglected, but, unlike STDA and SRPA, the EMPM offers the possibility to completely remove c.m. admixtures.

DOI: 10.1103/PhysRevC.107.014305

I. INTRODUCTION

The random phase approximation (RPA) has become the canonical approach to study the collective response of nuclei to external probes [1,2]. It provides a satisfactory description of the gross features of collective modes, such as their centroid energy and total strength, and as a linear-response theory it is generally preferred over the simpler Tamm-Dancoff approximation (TDA). However, in order to describe more detailed properties, like fragmentation and damping of giant resonances (GR) beyond the Landau mechanism, it is necessary to go beyond the harmonic approximation underlying the RPA method and couple the particle-hole (p-h) states building up the RPA phonons to more complex configurations.

The earliest extensions were achieved within the particle-vibration coupling (PVC) [3] and quasiparticle-phonon models (QPM) [4]. The QPM adopts a separable interaction to generate quasiparticle RPA (QRPA) phonons and couples them to two and, in some cases, three RPA phonon configurations to describe low- and high-energy collective modes [5].

In its first formulation [6], the PVC had a phenomenological character and was focused mainly on the fragmentation and damping of GR. It was then linked to energy density functional (EDF) theories and reformulated microscopically through the use of Skyrme interactions [7]. The same connection was established within the Green function (GF) framework based on the time blocking approximation (TBA) where the PVC emerges from nonrelativistic [8] and relativistic [9–11] EDF. Density dependent effective interactions derived from non-relativistic EDF, like Skyrme and Gogny, were also used in second RPA (SRPA) [12,13].

The SRPA, which also has a long history [14], is the most straightforward RPA extension. It solves directly the eigenvalue problem in a space spanned by p-h plus 2p-2h basis states. An example is provided by the calculations [15,16] performed by using a potential obtained through the unitary correlation operator method (UCOM) [17]. An even simpler approach is the second Tamm-Dancoff approximation (STDA) which is obtained from SRPA if the correlated ground state is replaced by the Hartree-Fock (HF) vacuum from the beginning, which in practice means that only the forward p-h and 2p-2h amplitudes are retained.

The RPA extensions based on the phenomenological EDF theories have to deal with a double counting problem. By going beyond the mean-field approximation, correlations already present in the ground state may be induced since the parameters of the EDF are determined so as to reproduce the ground state properties within HF. In order to avoid such a redundancy it is necessary either to redetermine the parameters or to adopt the so-called subtraction method proposed by Tselayev within the GFTBA [18,19] and used also within the SRPA [12].

*Corresponding author: Frantisek.Knapp@mff.cuni.cz

Another direct approach to the nuclear response is provided by the equation of motion phonon method (EMPM) [20,21]. In its upgraded formulation [22], the TDA phonons are the basic constituents of an orthonormal basis of n-phonon ($n = 2, 3, 4, \ldots$) states generated from solving iteratively a set of equations of motion in each n-phonon subspace. These states together with the HF state ($n = 0$) and the TDA phonons ($n = 1$) are adopted to solve the full eigenvalue problem. The method was also formulated in the quasiparticle language suitable for open shell nuclei [23] and in the p(h)-phonon scheme for the study of odd-nuclei [24–29].

The EMPM does not rely on any approximation except for the truncation of the configuration space and the number of phonons. Therefore, we should expect that, within a space including up to the two-phonon subspace, it should yield exactly the same results one obtains in STDA. This check represents the preliminary goal of the present work.

In order to make a consistent comparison between the three different approaches, we neglect the coupling between HF and two-phonon states in the EMPM, as it is the case in STDA. Such a coupling is implicit in RPA and SRPA since the Hamiltonian matrix is constructed by assuming that basis states are built on top of the correlated ground state. However, only excitation properties are calculated by construction, while the unperturbed HF wave function is used in the actual evaluation of the matrix elements.

The scope of our study is wider. We intend to put on display analogies and differences between the three formalisms and to investigate if and how their specific features impact on their performances. To this purpose, we will adopt the same states using the unitary correlation method (UCOM) two-body Hamiltonian throughout this work to determine the multipole response in some selected doubly magic nuclei.

We will pay special attention to the problem of the center of mass (c.m.) which may become critical once we go beyond the mean-field approximation. In fact, we know that the decoupling between intrinsic and c.m. motion is achieved in RPA if a HF basis in a complete or large enough p-h space is adopted [30], while in SRPA this is generally not true in spite of Thouless's theorem [30,31], because the stability condition is violated [32]. Recently, the c.m. contamination of the dipole spectrum was studied in extended RPA models based on the time blocking approximation (TBA) [33]. In TDA, the decoupling is obtained by exploiting the Gram-Schmidt orthogonalization method [34]. In the EMPM the c.m. spurious admixtures can be removed from the whole multiphonon basis under no constraint and for any single-particle (s.p.) basis by a method which exploits the singular value decomposition (SVD) [35,36]. The comparison between the three approaches will enable us to establish the role of the c.m. motion on the different multipole responses and how important is the removal of such a motion.

II. SHORT OUTLINE OF THE METHODS

A. STDA and SRPA

The SRPA eigenvalue equations are

$$\begin{pmatrix} \mathcal{A} & \mathcal{B} \\ -\mathcal{B}^* & -\mathcal{A}* \end{pmatrix} \begin{pmatrix} \mathcal{X}_\nu \\ \mathcal{Y}_\nu \end{pmatrix} = \omega_\nu \begin{pmatrix} \mathcal{X}_\nu \\ \mathcal{Y}_\nu \end{pmatrix}.$$

Here,

$$\mathcal{A} = \begin{pmatrix} A_{11} & A_{12} \\ A_{21} & A_{22} \end{pmatrix}, \quad \mathcal{B} = \begin{pmatrix} B_{11} & 0 \\ 0 & 0 \end{pmatrix}$$

and

$$\mathcal{X}_\nu = \begin{pmatrix} X_\nu^{(1)} \\ X_\nu^{(2)} \end{pmatrix}, \quad \mathcal{Y}_\nu = \begin{pmatrix} Y_\nu^{(1)} \\ Y_\nu^{(2)} \end{pmatrix},$$

where the labels 1 and 2 refer to the p-h and the 2p-2h subspaces and X and Y are the forward and backward amplitudes. Concerning the submatrices, $A_{11} = \{\langle i|H|j\rangle\}$ ($i = \text{ph}$, $j = \text{p}'\text{h}'$) is just the TDA Hamiltonian matrix, $A_{22} = \{\langle ij|H|kl\rangle\}$ are the matrix elements of the Hamiltonian in the 2p-2h subspace, $A_{12} = \{\langle i|H|jk\rangle\}$ provides the p-h to 2p-2h coupling, and $B_{11} = \{\langle 0|H|ij\rangle\}$ is the RPA coupling to the ground state. The other nondiagonal blocks vanish ($B_{12} = B_{21} = B_{22} = 0$) because they are evaluated using the HF vacuum instead of the correlated ground state and with only a two-body Hamiltonian [31,37]. The solution of the above equations yields the eigenvalues $\omega_\nu = E_\nu - E_0$, where E_0 is the ground-state energy, E_ν are energies of the eigenstates

$$|\Psi_\nu\rangle = \left(\mathcal{O}_\nu^{(1)} + \mathcal{O}_\nu^{(2)}\right)|0\rangle, \tag{1}$$

where

$$\mathcal{O}_\nu^{(1)} = \sum_i \left[X_\nu^{(1)}(i) q_1^\dagger(i) - Y_\nu^{(1)}(i) q_1(i)\right]$$
$$\mathcal{O}_\nu^{(2)} = \sum_{ij} \left[X_\nu^{(2)}(ij) q_2^\dagger(ij) - Y_\nu^{(2)}(ij) q_2(ij)\right]. \tag{2}$$

Here, $q_1^\dagger(q_1)$ and $q_2^\dagger(q_2)$ create (destroy) p-h (i) and 2p-2h (ij) states, respectively.

If we put $B_{11} = 0$ (no ground state correlations), we obtain the STDA equations

$$\mathcal{A}\mathcal{X}_\nu = \omega_\nu \mathcal{X}_\nu \tag{3}$$

whose eigenstates are simply of the form

$$|\Psi_\nu\rangle = \left[\sum_i X_\nu^{(1)}(i) q_1^\dagger(i) + \sum_{ij} X_\nu^{(2)}(ij) q_2^\dagger(ij)\right]|0\rangle. \tag{4}$$

B. EMPM

The EMPM goes through three steps. We first map the p-h configurations into a TDA phonon basis

$$\{|\text{ph}\rangle\} \to \{|\lambda\rangle\} = \{O_\lambda^\dagger|0\rangle\}. \tag{5}$$

Starting from the TDA one-phonon states $|\alpha_1\rangle = |\lambda\rangle$, we generate iteratively an orthonormal basis of n-phonon ($n = 2, 3 \ldots$) correlated states $|\alpha_n\rangle$ through various steps. Assuming known the $(n-1)$-phonon basis states $|\alpha_{n-1}\rangle$, we construct n-phonon states

$$|i\rangle = |\lambda\alpha_{n-1}\rangle = O_\lambda^\dagger|\alpha_{n-1}\rangle. \tag{6}$$

From this redundant set we extract a basis of linearly independent (but not orthogonal) states through the Cholesky decomposition method and formulate, in the basis so obtained,

the generalized eigenvalue equation within the n-phonon subspace

$$\sum_{jk}\left(\mathcal{A}^{(n)}_{ik} - E^{(n)}\delta_{ik}\right)\mathcal{D}^{(n)}_{kj}C^{(n)}_{j} = 0. \tag{7}$$

In Eq. (7)

$$\mathcal{D}^{(n)}_{ij} = \langle i \mid j\rangle \tag{8}$$

is the overlap or metric matrix and

$$\mathcal{A}^{(n)}_{ij} = E_i\delta_{ij} + \mathcal{V}^{(n)}_{ij}, \tag{9}$$

where E_i is the unperturbed energy of the n-phonon state (6). The formulas giving the overlap matrix $\mathcal{D}$ and the phonon-phonon interaction $\mathcal{V}$ can be found, for instance, in Ref. [38].

The solution of Eq. (7) yields an orthonormal basis of states

$$|\alpha_n\rangle = \sum_{\lambda\alpha_{(n-1)}} C^{\alpha_n}_{\lambda\alpha_{(n-1)}}|\lambda\alpha_{(n-1)}\rangle \tag{10}$$

within the n-phonon subspace. The iteration of the procedure up to an arbitrary n produces a set of states which, added to HF ($|0\rangle$) and TDA ($\{|\alpha_1\rangle\} = \{|\lambda\rangle\}$), form an orthonormal basis $\{|\alpha_n\rangle\}$ ($n = 0, 1, 2, 3, ...$) with energies E_{α_n}, spanning the full multiphonon space.

In such a space, we solve the final eigenvalue equations

$$\sum_{\alpha_n\beta_{n'}}((E_{\alpha_n} - \mathcal{E}_\nu)\delta_{\alpha_n\beta_{n'}} + \mathcal{V}_{\alpha_n\beta_{n'}})\mathcal{C}^\nu_{\beta_{n'}} = 0, \tag{11}$$

where $\mathcal{V}_{\alpha_n\beta_{n'}} = 0$ for $n' = n$. The formulas giving $\mathcal{V}_{\alpha_n\beta_{n'}}$ ($n' \neq n$) can be found in Ref. [36]. The resulting eigenvectors (with corresponding energies $\mathcal{E}_\nu$)

$$|\Psi_\nu\rangle = \sum_{n,\alpha_n}\mathcal{C}^\nu_{\alpha_n}|\alpha_n\rangle, \tag{12}$$

including the ground state $|\Psi_0\rangle$, are fully correlated. In order to make a comparison with the other two approaches we consider a space including up to two phonons and neglect the coupling between the HF vacuum and the two-phonon states ($\langle\alpha_2|H|0\rangle = 0$). As already pointed in the introduction, such a coupling is absent in STDA, while it is implicit in SRPA excited states. Under this assumption, the excited states have the structure

$$|\Psi_\nu\rangle = \sum_\lambda \mathcal{C}^\nu_\lambda|\lambda\rangle + \sum_{\lambda_1\lambda_2}\mathcal{C}^\nu_{\lambda_1\lambda_2}|\lambda_1\lambda_2\rangle, \tag{13}$$

where we made use of Eq. (10).

C. Comparative analysis

We have seen already that SRPA turns into STDA if one neglects the ground state correlations which in SRPA are treated in the quasiboson approximation. Within the p-h + 2p-2h space, the EMPM wave functions (13) can assume the structure of the STDA states (4) by expressing the TDA phonons λ in terms of the p-h configurations. Since there is a one to one correspondence between p-h and TDA states, the EMPM is completely equivalent to STDA. We will demonstrate it on many numerical examples in the next section.

With respect to both STDA and SRPA, the EMPM adopts a correlated basis which can be safely truncated. Moreover, it allows naturally the extension of the calculations beyond 2p-2h in spaces including three-phonon and, even, four-phonon states and yields an explicitly correlated ground state without resorting to any approximation apart from a space truncation.

The EMPM has the disadvantage that it has to deal with a redundant basis which renders the procedure more involved. On the other hand, just the use of such a basis allows a complete and exact elimination of the spurious admixtures induced by the c.m. motion for any single-particle basis. In fact, we can first generate a basis of c.m. free TDA states orthogonal to the c.m. spurious state $|\lambda_{\text{c.m.}}\rangle$ by applying the Gram-Schmidt orthogonalization to the p-h configurations [34]. The SVD allows us to extend the orthogonalization procedure to all n-phonon subspace [35]. For $n = 2$, for instance, we distinguish the set of spurious states $\{|i_{\text{c.m.}}\rangle\} = \{|\lambda\lambda_{\text{c.m.}}\rangle, |\lambda_{\text{c.m.}}\lambda_{\text{c.m.}}\rangle\}$ from the other two-phonon states $\{|j\rangle\} = \{|\lambda\lambda'\rangle\}$.

The SVD method decomposes the rectangular overlap matrix

$$\mathcal{D}_{j,i_{\text{c.m.}}} = \langle i_{\text{c.m.}} \mid j\rangle \tag{14}$$

into two mutually orthogonal diagonal blocks defining two subspaces. One is spanned by the c.m. free basis $\{|\alpha\rangle\}$, the other by the c.m. spurious states $\{|\alpha_{\text{c.m.}}\rangle\}$. The two subspaces are mutually orthogonal

$$\langle\alpha_{\text{c.m.}} \mid \alpha\rangle = 0. \tag{15}$$

The procedure can be extended to any n-phonon subspace ($n = 3, 4, \ldots$).

We will investigate how the differences between the three approaches and, especially, the different treatment of the c.m. motion have a quantitative impact on the nuclear multipole responses. To our knowledge, only in RPA are the physical excited states automatically decoupled from the spurious c.m. motion.

III. NUMERICAL IMPLEMENTATION AND RESULTS

We adopt an intrinsic Hamiltonian of the form

$$H = T_{\text{int}} + V = \sum_{i<j}\left(\frac{\mathbf{p}^2_{ij}}{2Am} + V_{ij}\right), \tag{16}$$

where $\mathbf{p}_{ij} = \mathbf{p}_i - \mathbf{p}_j$ and m is the nucleon mass, for both protons and neutrons. We adopt the UCOM potential [17] to generate a HF basis from a HO model space truncated in the major oscillator quantum number $N_{\max} = 6$ and the oscillator length $b = 1.7$ fm. Being derived from Argonne V18 [39], UCOM can be considered a realistic two-body potential which avoids the double-counting problems affecting entirely phenomenological potentials [18,19]. We include in the construction of S(TDA), S(RPA) matrices all the HF single particle, 1p-1h, and 2p-2h basis states allowed by the HO space. Correspondingly, all the TDA phonons to build the two-phonon basis are used in EMPM.

We will compute the strength functions of the electric multipole operators whose general form is

$$\mathcal{M}(E;\lambda\mu) = \sum_k e_k r_k^{(\lambda+n)}Y_{\lambda\mu}(\hat{k}), \tag{17}$$

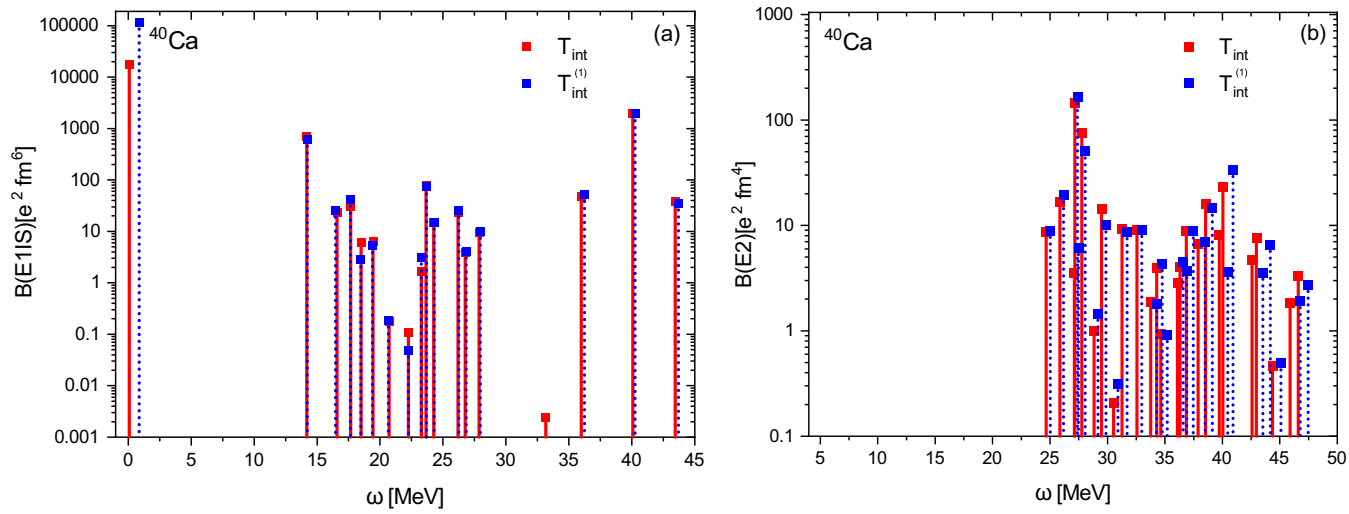

FIG. 1. $E1$ (a) and $E2$ (b) responses of ^{40}Ca evaluated in RPA with the intrinsic two-body kinetic energy operator $T_{\rm int}$ ("intrinsic") and with the effective one-body kinetic energy operator $T^{(1)}_{\rm int}$ ("effective").

where, unless specified otherwise, we use the bare charges, $e_k = e$ for protons and $e_k = 0$ for neutrons, while n is specified below depending on the multipole case.

The strength function is given

$$S(E\lambda, \omega) = \sum_\nu B(E\lambda, \Psi_0 \to \Psi_\nu)\delta(\omega - \omega_\nu), \tag{18}$$

where $\omega_\nu = E_\nu - E_0$ and

$$B(E\lambda, \Psi_0 \to \Psi_\nu) = |\langle \Psi_\lambda \| \mathcal{M}(E\lambda) \| 0 \rangle|^2 \tag{19}$$

is the reduced transition probability. We will replace the δ function with a Lorentzian

$$\delta(\omega - \omega_\nu) \to \frac{1}{2\pi} \frac{\Gamma}{(\omega - \omega_\nu)^2 + \Gamma^2/4} \tag{20}$$

of width $\Gamma = 0.5$ MeV for presentation purposes.

The choice of the intrinsic Hamiltonian, Eq. (16), specifically, of the intrinsic two-body operator for the kinetic energy, is relevant in what follows. To some extent, the c.m. kinetic energy can be subtracted by employing the same form as the total kinetic-energy operator, which is a single-particle operator, but with a correction to the nucleon mass,

$$T^{(1)}_{\rm int} = \left(1 - \frac{1}{A}\right) \sum_{i=1}^{A} \frac{\mathbf{p}_i^2}{2m}. \tag{21}$$

This prescription is often used in RPA calculations based on phenomenological functionals [40]. However, with such choice, the formal conditions for the spurious state to appear at zero energy are not met. Let us consider, for example, the spurious c.m. motion operator $O_{sp} = \frac{1}{A}\sum_{i=1}^{A} \vec{r}_i$, which contaminates the dipole channel. As pointed out also in Ref. [32] for the total kinetic energy, $T^{(1)}_{\rm int}$ does not commute with O_{sp}, so the total energy weighted sum rule does not vanish. As a result, all RPA calculations employing $T^{(1)}_{\rm int}$ produce a spurious state at an energy of finite value (real or imaginary), regardless of how large the p-h space is. By contrast, $T_{\rm int}$ does commute with O_{sp} and RPA implementations employing it can produce a spurious state at practically zero energy (in terms of the numerical precision of the overall implementation). As a demonstration, we compare in Fig. 1 RPA results obtained with $T_{\rm int}$, i.e., by employing the Hamiltonian of Eq. (16), and with $T^{(1)}_{\rm int}$, Eq. (21). Specifically, we show the RPA response of ^{40}Ca to the isoscalar dipole operator given by Eq. (17) with $\lambda = 1, n = 2, e_p = e_n = e$. Here, we use the c.m. uncorrected form of the transitions operator in order to emphasize the position and the strength of the spurious state.

In the case of $T_{\rm int}$, even in such a small basis ($N_{\rm max} = 6$ or 60 p-h states) the spurious state occurs at 0.09 MeV. In the case of $T^{(1)}_{\rm int}$, it appears at 0.86 MeV. The respective values in a basis of $N_{\rm max} = 10$ are 0.006 and 0.322 MeV. All eigenstates are affected by the choice of kinetic-energy operator and the same holds in all channels as exemplified in the quadrupole case, also shown in Fig. 1.

A. Nuclear response in ^{16}O and ^{40}Ca

1. Isovector electric dipole response

For the isovector electric dipole operator, $n = 0$ and $\lambda = 1$ in Eq. (17), we replace the bare charges with the effective ones $e_k = (N/A)e$ for protons and $e_k = -(Z/A)e$ for neutrons in order to minimize the impact of the c.m. coordinates. They are obtained by referring the nucleonic coordinates to the c.m. coordinate, $\vec{r}_k \to (\vec{r}_k - \vec{R}_{\rm c.m.})$. Such a replacement would be unnecessary within the EMPM. In fact, after the SVD treatment, we obtain the same strengths whether we use bare or effective charges.

The behavior of $E1$ strength functions is very similar in both ^{16}O and ^{40}Ca (Fig. 2). As shown in panels (a) and (d), the use of the effective charges ensures the complete removal of the c.m. admixtures in RPA and, to a very large extent, in TDA. In the latter case, the residual impurity is removed after the implementation of the Gram-Schmidt orthogonalization procedure. Remarkably enough, TDA and RPA strength functions are practically indistinguishable.

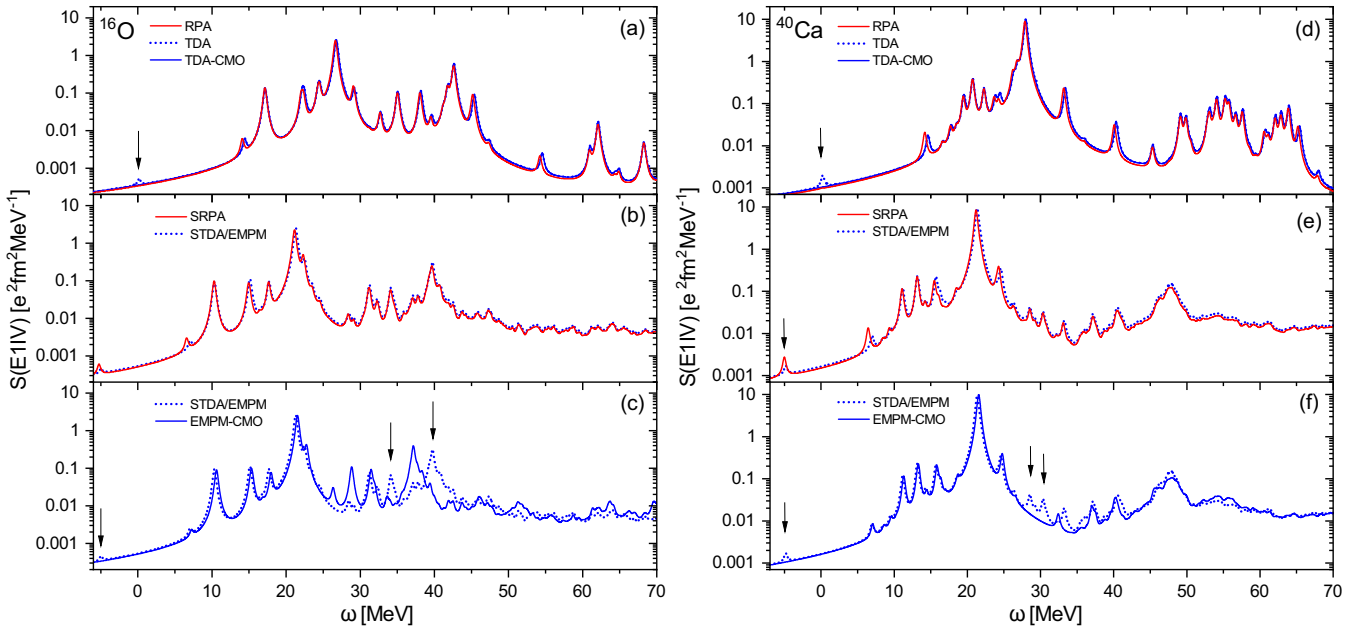

FIG. 2. Isovector $E1$ strength functions in ^{16}O and ^{40}Ca in different approaches. The TDA strength is computed before (TDA) and after the application of Gram-Schmidt c.m. orthogonalization procedure (TDA-CMO). In this and the following figures, a single line is drawn for STDA and EMPM since they yield identical results. The arrows indicate states with significant spurious components which disappear if c.m. SVD orthogonalization procedure (EMPM-CMO) is applied.

Panels (b) and (e) show that the STDA strength distribution is identical to the one computed within the EMPM before the implementation of the SVD. Both strengths are nearly indistinguishable from the one obtained in SRPA.

The implementation of the SVD method has a visible effect [panels (c) and (f)]. It identifies and removes three spurious peaks, present in all approaches, one at negative energy and two at high energy. However, it does not alter significantly the overall profile of the strength, especially in the region of the giant dipole resonance.

2. Isoscalar dipole response

For the isoscalar dipole response we use the operator

$$\mathcal{M}_{IS}(E;1\mu) = e\sum_k \left(r_k^2 - \frac{5}{3}\langle r^2\rangle\right) r_k Y_{1\mu}(\hat{k}). \qquad (22)$$

The linear term is introduced in order to minimize the spurious contributions coming from the c.m. motion. The strength function for ^{16}O and for ^{40}Ca is shown in Fig. 3. In analogy with the case of the isovector $E1$ transitions, the TDA and STDA isoscalar $E1$ strength distributions overlap to a very large extent with the RPA and SRPA corresponding distributions, respectively. Despite the inclusion of the linear term in Eq. (22), a spurious peak occurs at zero energy in RPA and, especially, in TDA [panels (a) and (d)]. In TDA, it disappears after the Gram-Schmidt orthogonalization. As we move to STDA and SRPA [panels (b) and (e)], we observe that the low-lying spurious peak remains and drops to negative energy. The implementation of the SVD method not only eliminates such a peak but reveals and eliminates two additional spurious peaks. More in general, it shows that, if not eliminated, the spuriousness spreads over fairly large energy intervals and alters portions of the profile of the strength distribution [panels (c) and (f)].

3. Monopole and quadrupole responses

From comparing Figs. 4 and 5 we observe that monopole ($n = 2$ and $\lambda = 0$) in Eq. (17) and quadrupole ($n = 0$ and $\lambda = 2$) responses exhibit similar characteristics in ^{16}O. We notice a near overlap between TDA and RPA [panel (a)] as well as between STDA and SRPA [panel (b)] strength distributions, especially in the quadrupole case. Humps at zero energy appear in both STDA and SRPA. Such peaks are induced by the c.m. motion through $[1^- \otimes 1^-]^{0^+,2^+}$ coupling of the spurious state with itself. The c.m. spuriousness is not concentrated only around zero energy but spreads over the whole energy interval. It generates several spurious peaks, in addition to the zero energy one, and contaminates other transitions. All spurious peaks as well the contaminations of other transitions are eliminated once the SVD method is implemented.

Figures 4 and 5 show that the features of the monopole and quadrupole responses in ^{40}Ca are very similar to those observed in ^{16}O. The only significant discordance is that in ^{40}Ca, the zero energy spurious monopole and quadrupole peaks appear in STDA but not in SRPA. The reason is that the SRPA energy eigenvalues corresponding to these peaks are imaginary. Implementation of the SVD method removes not only the zero energy bumps but also all states with spurious admixtures.

4. Octupole response

The TDA and RPA octupole [$n = 0$ and $\lambda = 3$ in Eq. (17)] strength distributions overlap over a large interval at high

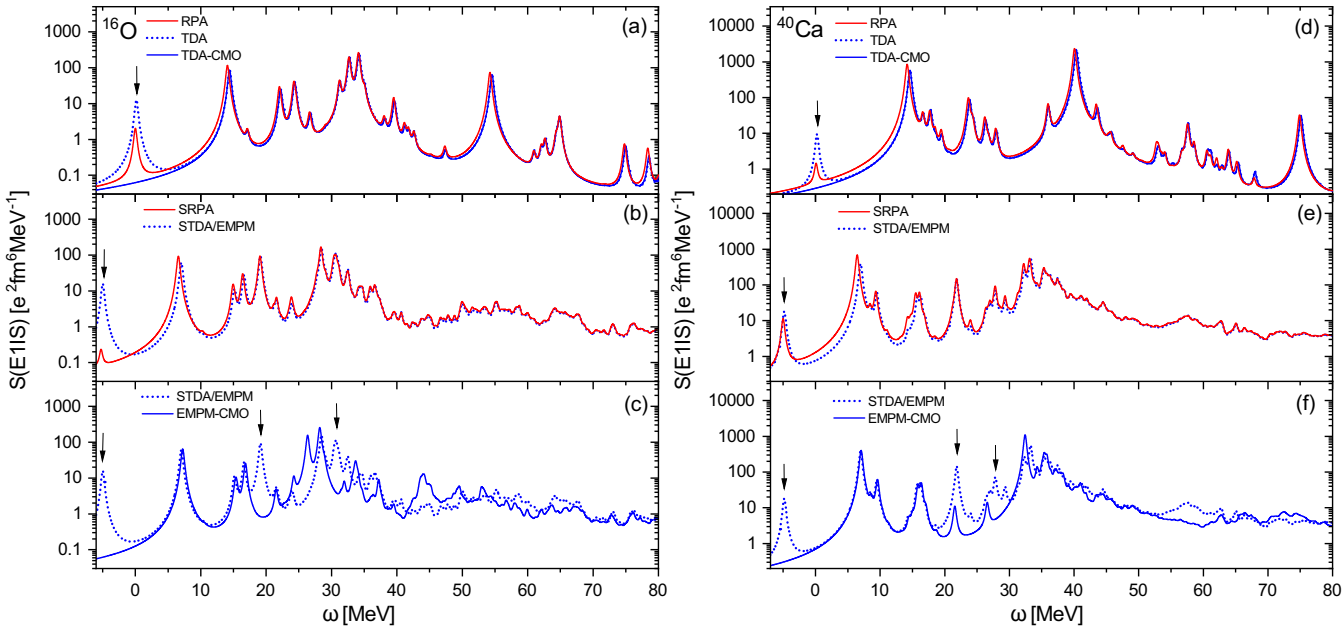

FIG. 3. Isoscalar $E1$ strength functions in ^{16}O and ^{40}Ca.

energy but differ considerably from each other in the low energy sector [Figs. 6(a) and 6(d)]. Both approaches yield a strong low energy peak. However, the one obtained in RPA is more than 5 MeV below in energy and disappears in SRPA [Figs. 6(b) and 6(e)] because it is obtained at imaginary energy. In STDA (EMPM) such a low-lying peak is still present even after the implementation of the SVD method [Figs. 6(c) and 6(f)]. Therefore, it corresponds to a genuine physical resonance. The c.m. affects the spectrum only at high energy, above 20 MeV. SVD disposes of all spurious peaks as well as of the residual contaminations.

B. Nuclear response in ^{48}Ca

We examine ^{48}Ca separately from ^{16}O and ^{40}Ca as a qualitatively different system. Specifically, it is not only isospin asymmetric, but it also develops a low-lying quadrupole vibration which can couple to other phonons and affect all channels.

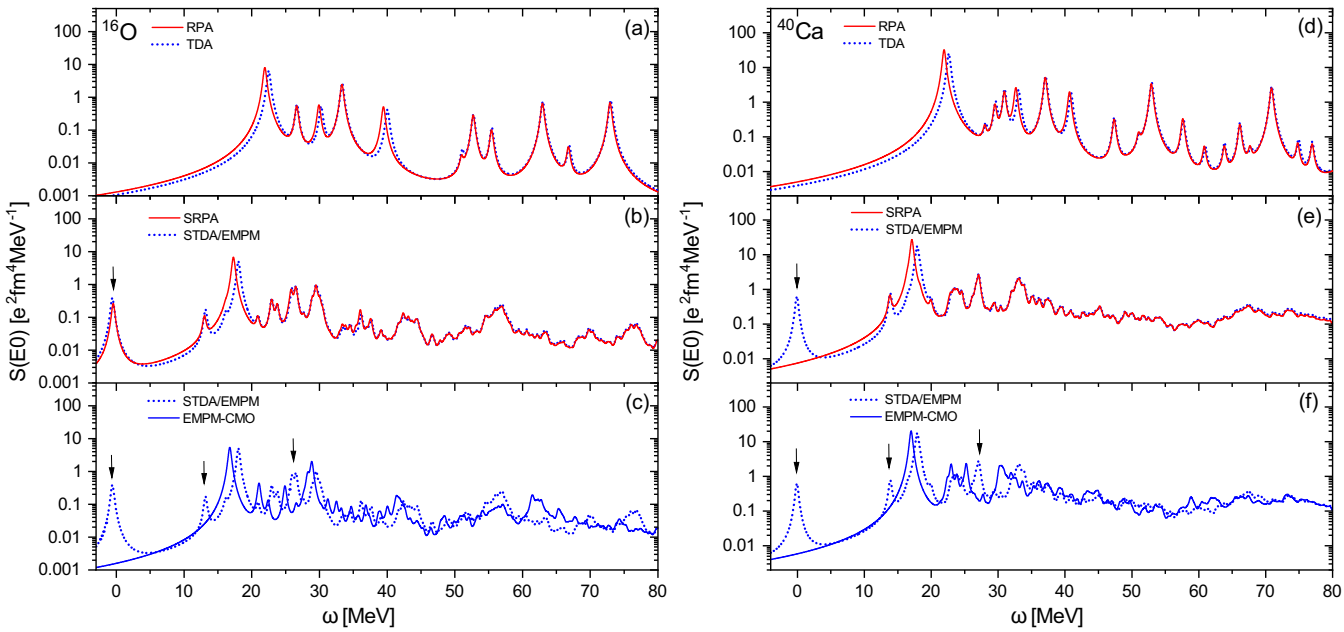

FIG. 4. Monopole strength functions in ^{16}O and ^{40}Ca.

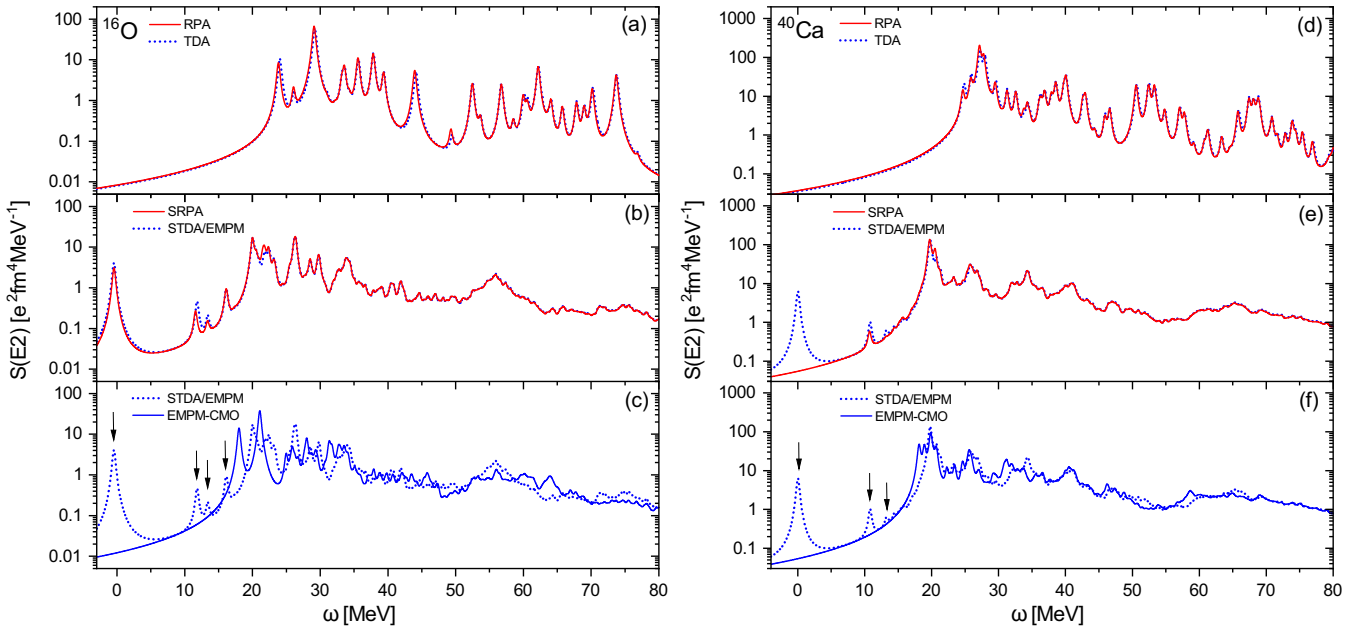

FIG. 5. Quadrupole strength functions in ^{16}O and ^{40}Ca.

As shown in Fig. 7, the isovector $E1$ response is very similar in both TDA and RPA as well as in STDA and SRPA. The c.m. induces a small peak in TDA and two weak transitions in STDA and SRPA. Its overall impact on the response is modest as shown in panel (c).

More pronounced is its effect on the isoscalar $E1$ strength function (Fig. 8). The c.m. motion generates several peaks and contaminates several transitions. All these impurities disappear after the SVD treatment.

TDA and RPA as well as STDA and SRPA have a similar $E3$ response at high energy (Fig. 9). At low energy, instead, important deviations are observed. The RPA low-energy peak is shifted by about 5 MeV with respect to TDA. In SRPA it is further shifted with respect to STDA. The SVD method removes a low-energy hump predicted by both STDA and SRPA and washes the residual spurious admixtures, which distort the spectrum in both the low- and high-energy part.

The quadrupole (Fig. 10) and monopole (Fig. 11) responses are similar in the high energy sector but behave differently at low energy. Both TDA and RPA yield two $E2$ low-energy peaks, while the monopole spectra are flat. A spurious monopole peak at zero energy appears in STDA

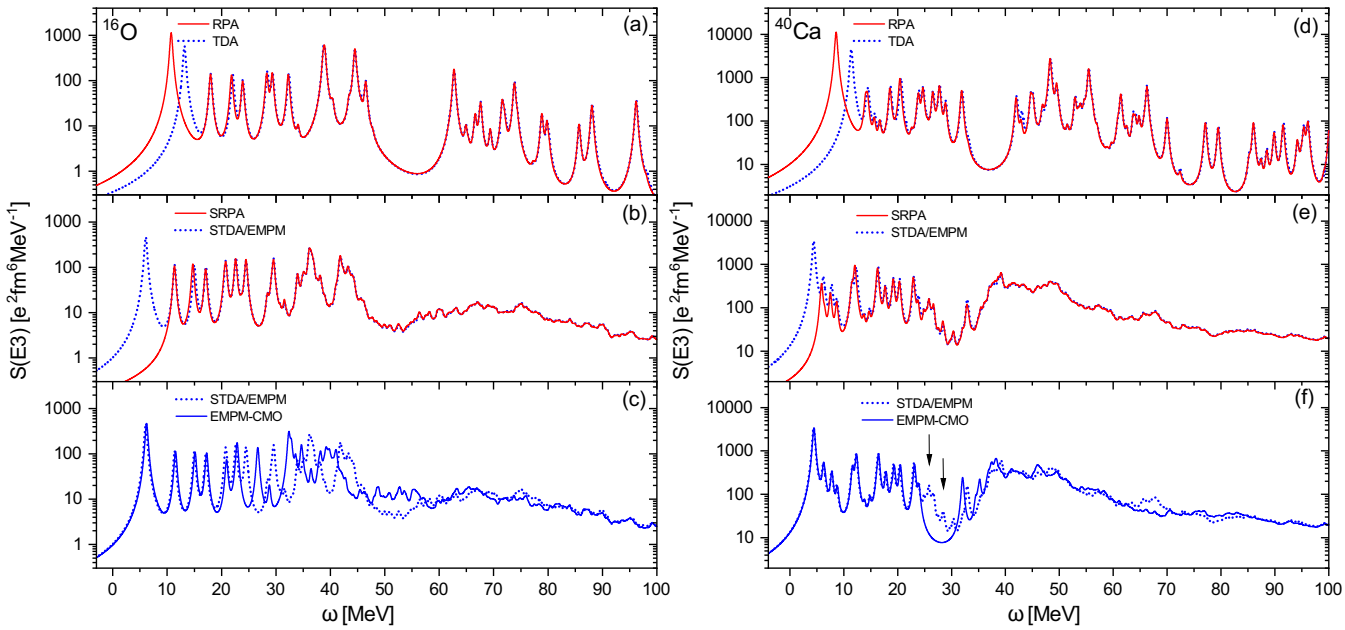

FIG. 6. $E3$ strength functions in ^{16}O and ^{40}Ca.

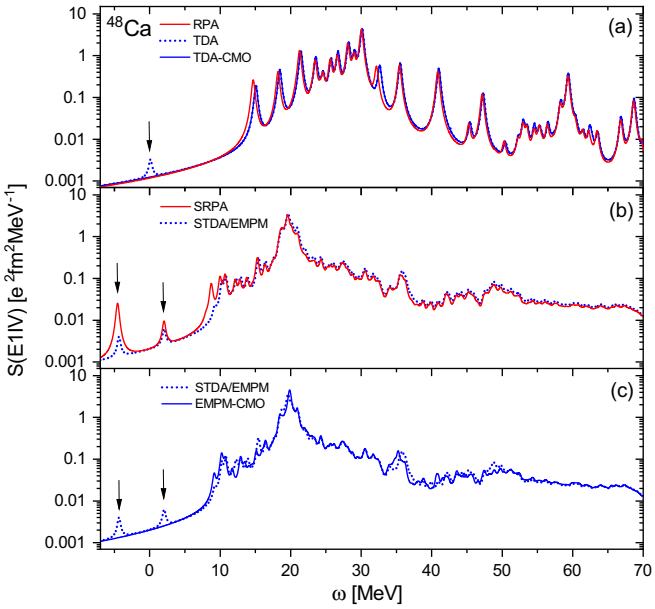

FIG. 7. Isovector $E1$ strength functions in ^{48}Ca.

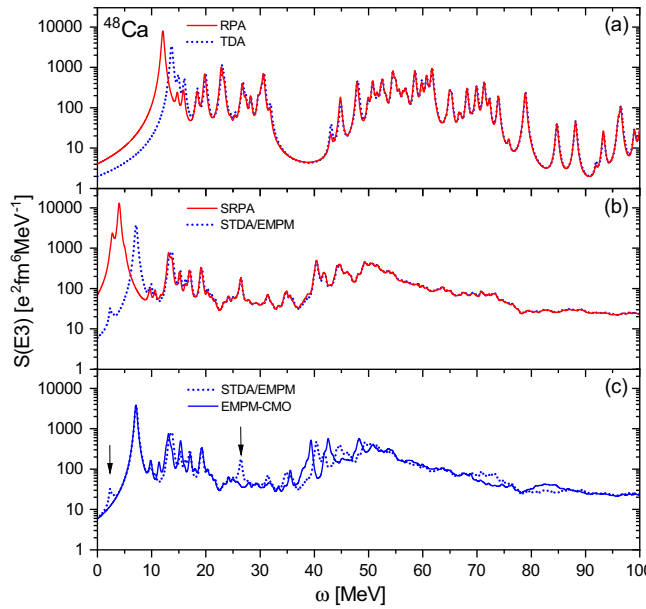

FIG. 9. $E3$ strength functions in ^{48}Ca.

(EMPM) but not in SRPA, again because of the imaginary nature of the corresponding energy eigenvalue. The discrepancy is solved once such a spurious excitation is removed through the SVD method. Three low energy quadrupole peaks are generated in STDA (EMPM) and two in SRPA. Two of the three peaks survive even after the implementation of SVD. They are genuine physical states.

However, the excitation energy of one of the two peaks is negative, in both STDA and SRPA, implying that the excited 2^+ state lies below the HF state. Such an anomaly indicates that, at least for the potential adopted here, it is not appropriate to consider the unperturbed HF as ground state, a tacit assumption made in RPA, SRPA, and STDA. We need to replace HF with a correlated ground state, but such a replacement would require the inclusion of 3p-3h, or three-phonon basis states. Such a task is beyond the scope of the present work.

C. Running sum

It is useful to analyze the nuclear response from the perspective offered by the running sum. Since RPA and SRPA fulfill the energy weighted sum rule (EWSR) [1,41], it is meaningful to refer the different sums to the RPA sum in order to determine to what extent they deviate from the EWSR.

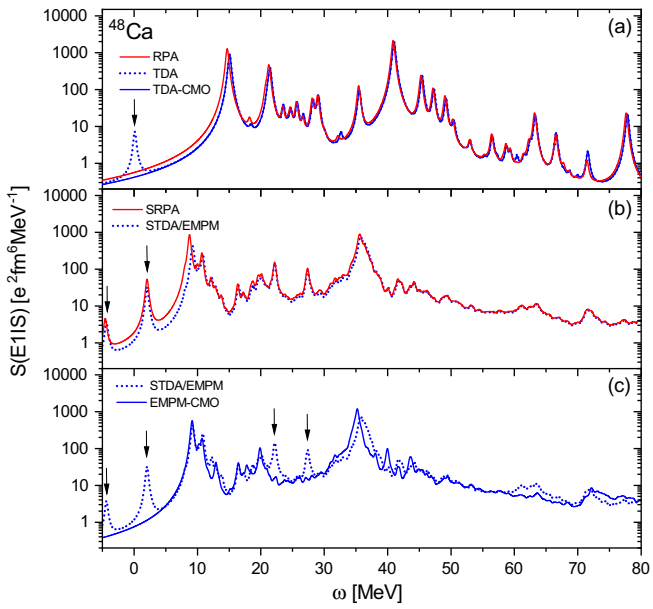

FIG. 8. Isoscalar $E1$ strength functions in ^{48}Ca.

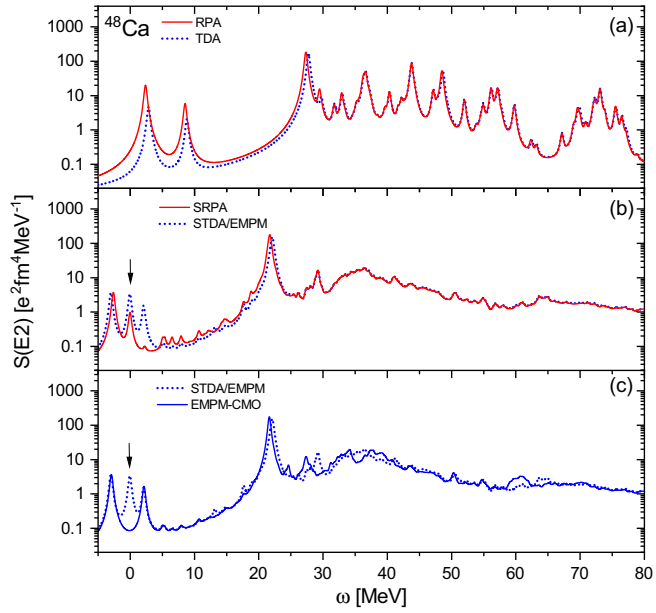

FIG. 10. Quadrupole strength function in ^{48}Ca.

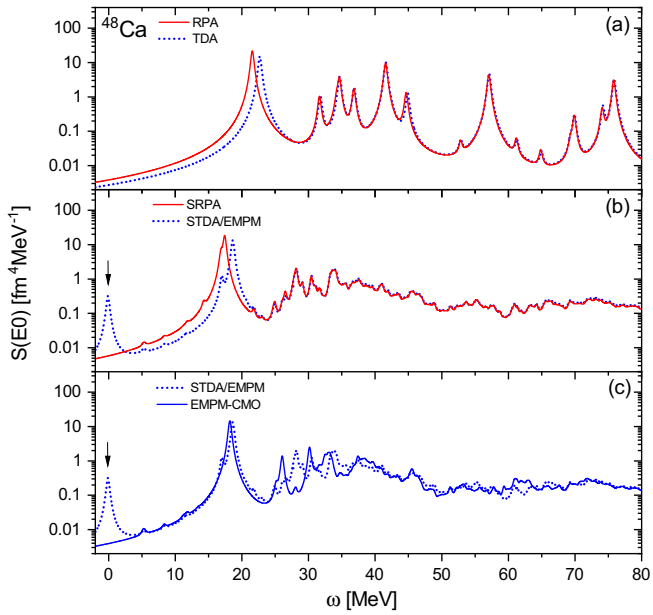

FIG. 11. Monopole strength function in ^{48}Ca.

Several interesting aspects emerge from examining the plots shown in Figs. 12–17. In all nuclei under investigations the running sums of all transitions, determined in TDA and STDA/EMPM follow closely, from below, the one evaluated in RPA and account almost entirely (from 90% to 95%) for the RPA EWSR. The only exception is the isovector $E1$, which overestimates the RPA sum by 10%. We can infer from these results that, in TDA and STDA/EMPM, the EWSR is underestimated in the isoscalar (attractive) channels and overestimated in the isovector (repulsive) channel, consistently with the schematic model [42]. This is what one should have expected since TDA and STDA/EMPM fulfill the nonenergy weighted sum rule (NEWSR). Indeed, we have checked that this is the case in our calculation.

Also the STDA/EMPM and the SRPA integrated strengths evolve closely. Their smooth evolution reflects the fragmentation of the strengths induced by the coupling to 2p-2h configurations. The STDA/EMPM running sum tends exactly to the TDA energy weighted sum. Analogously, in SRPA and RPA, the energy weighted sum coincides in most nuclei and for most multipolarities.

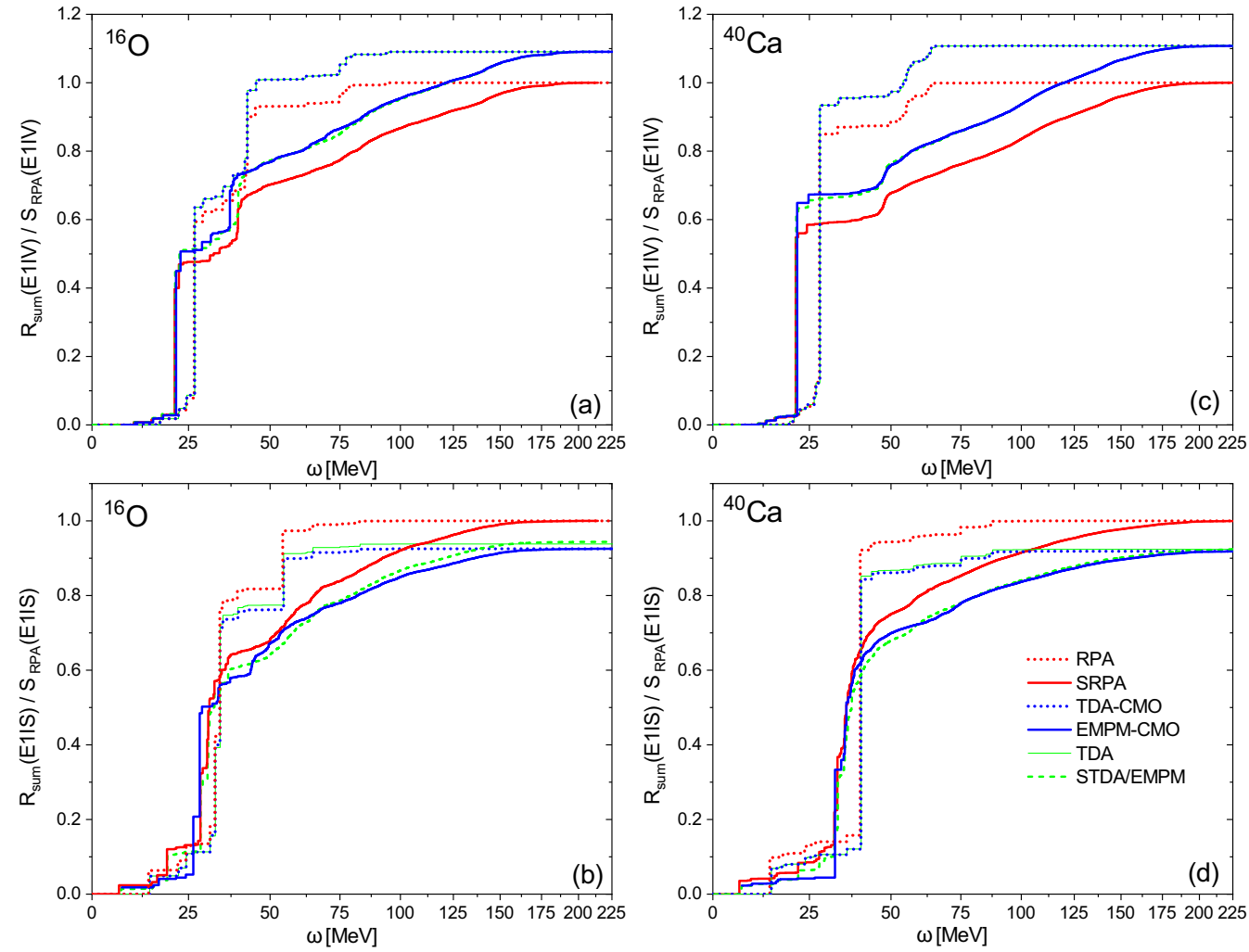

FIG. 12. Isovector and isoscalar $E1$ energy weighted running sums in ^{16}O and ^{40}Ca.

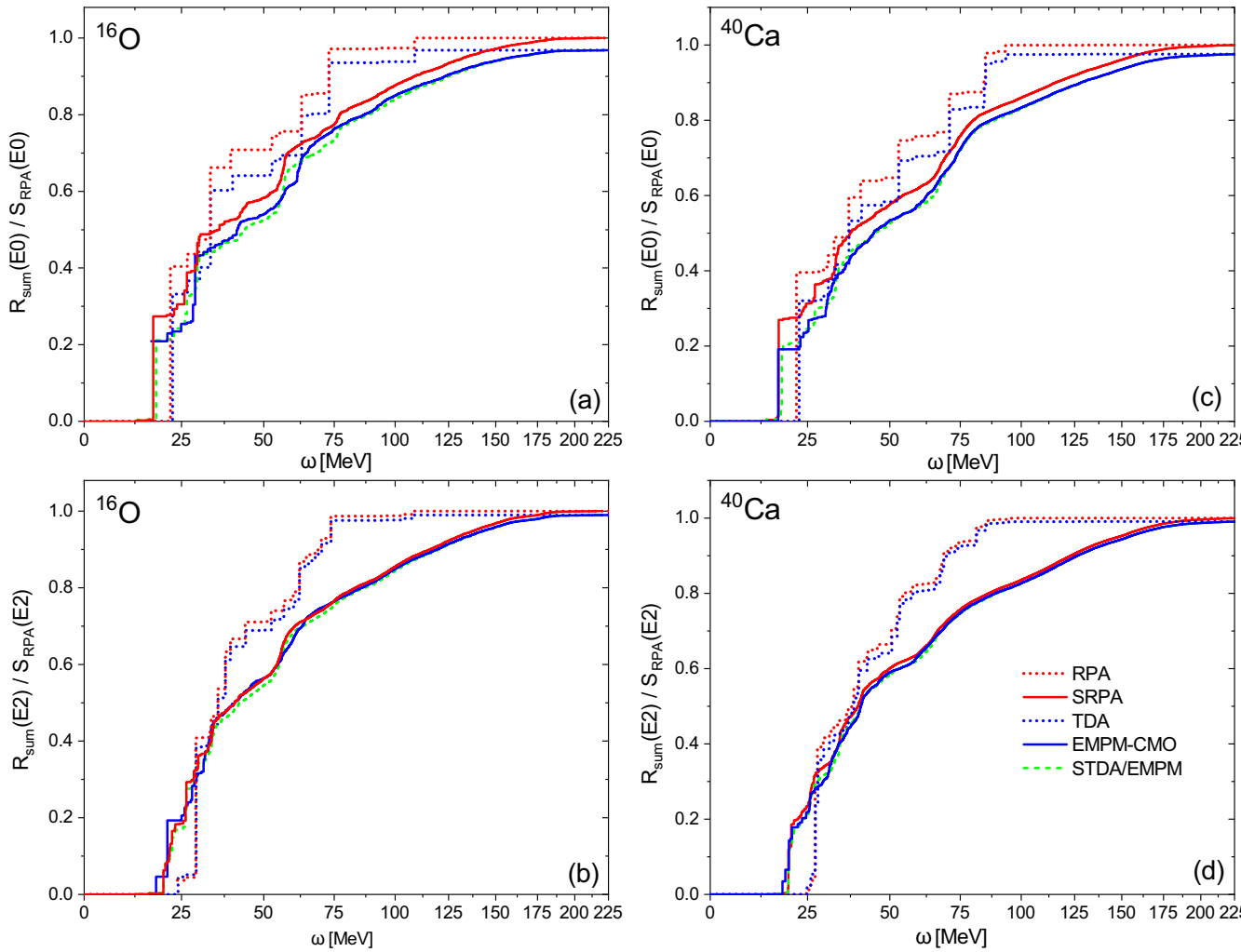

FIG. 13. $E0$ and $E2$ energy weighted running sums in ^{16}O and ^{40}Ca.

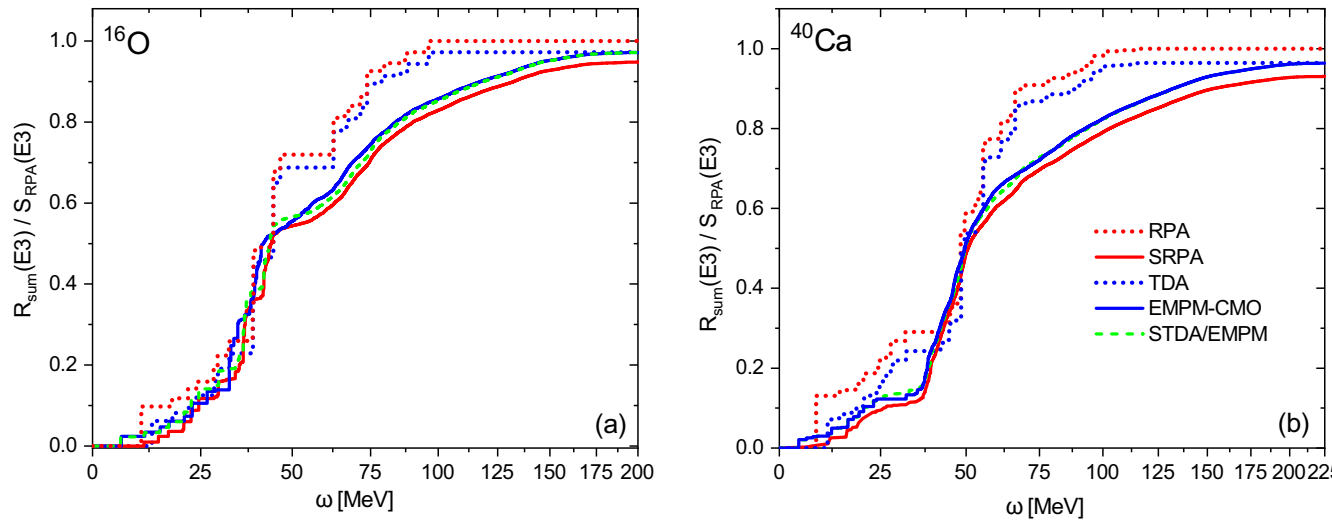

FIG. 14. $E3$ energy weighted running sums in ^{16}O and ^{40}Ca.

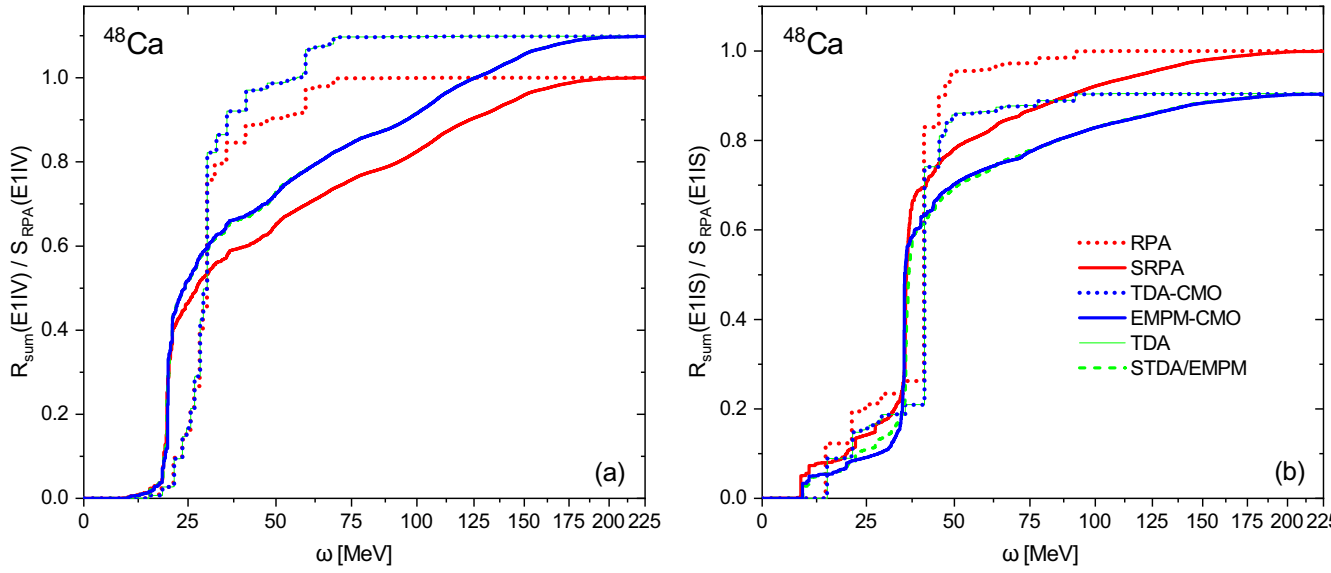

FIG. 15. Isovector and isoscalar $E1$ energy weighted running sums in ^{48}Ca.

There are some exceptions. In ^{40}Ca, the SRPA underestimates appreciably the RPA $E3$ EWS. The simple reason is that the lowest level which was supposed to carry a large $E3$ strength is imaginary. Another peculiarity of SRPA, which was discussed in Ref. [32], is that the RPA $E2$ EWS is preserved only if we include in the running sum the negative energy 2^+ level and its strength.

A final remark concerns the effect of the center of mass. The EWS of all multipolarity remains unaltered whether we remove or not the c.m. motion. Due to this invariance, the conservation of the EWS can provide valuable guidance in any beyond mean-field extension.

IV. CONCLUSION

From the present survey we can draw some clearcut conclusions. The differences between TDA and RPA as well as between STDA and SRPA responses are marginal, except for the octupole transitions where the RPA low-lying octupole peak is shifted considerably downward with respect to TDA. In going from RPA to SRPA, such a peak is pushed further down in energy and can disappear completely if the corresponding eigenvalue becomes imaginary. This instability casts a shadow on the reliability of approaches which are meant to go beyond RPA. SRPA then remains applicable primarily on higher-lying collective modes, i.e., giant res-

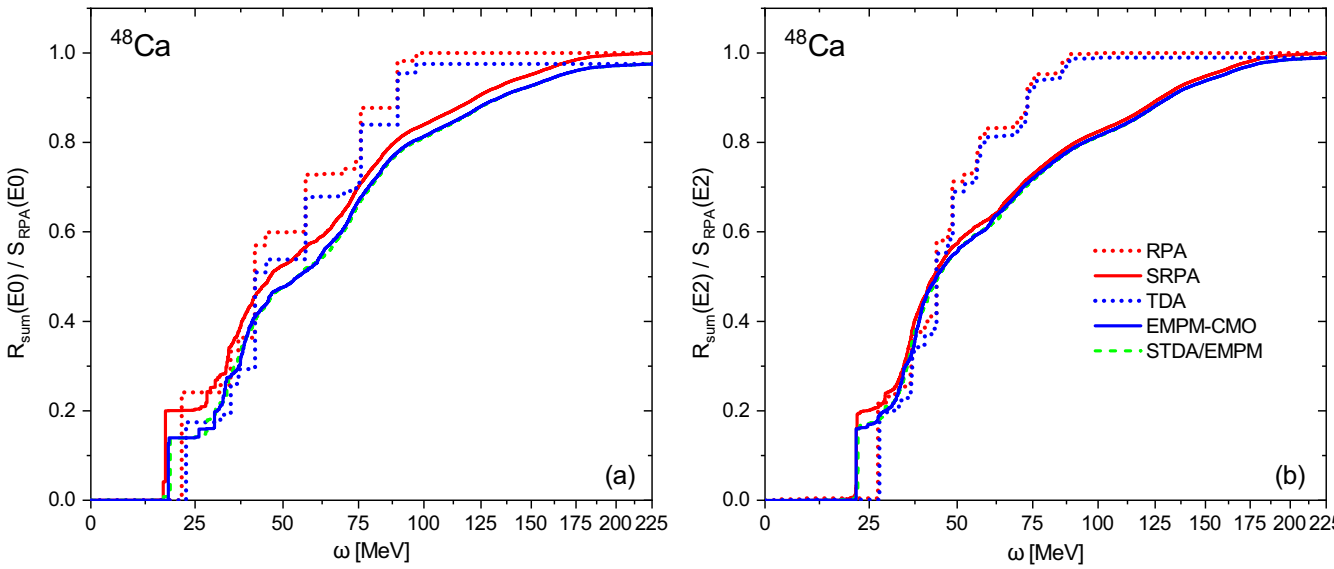

FIG. 16. $E0$ and $E2$ energy weighted running sums in ^{48}Ca.

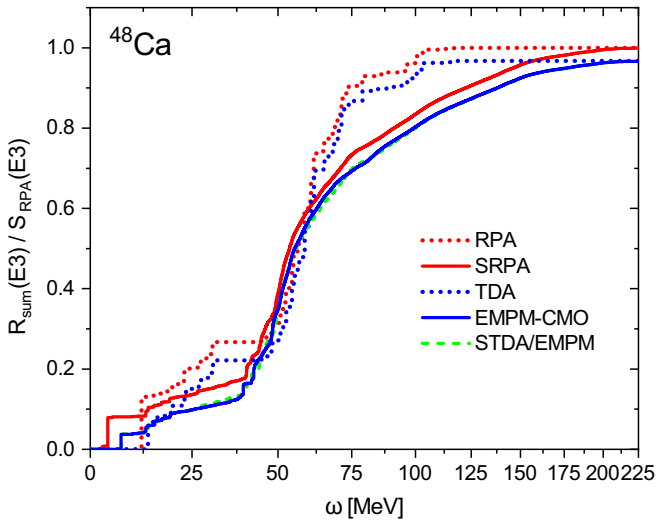

FIG. 17. $E3$ energy weighted running sums in ^{48}Ca.

onances. The TDA and STDA spectra do not exhibit any anomaly.

In RPA, it is possible to remove almost completely the low-lying spurious isovector $E1$ peak thanks to the adoption of a HF basis combined with the subtraction of the c.m. coordinates from the dipole operator. In TDA, the Gram-Schmidt orthogonalization procedure eliminates any spurious admixtures from both isoscalar and isovector responses.

In going to STDA and SRPA, however, the c.m. motion affects all multipoles. Its spuriousness spreads over the entire spectrum of each multipole thereby inducing non-negligible distortions of the isoscalar $E1$, $E2$, and $E3$ strength functions. Only the isovector $E1$ response is marginally affected.

STDA and SRPA do not offer any obvious recipe for removing these distortions, while in the EMPM the joint use of Gram-Schmidt and SVD pins down and removes completely and exactly the spurious admixtures from all multipole responses. In principle, the same orthogonalization procedure can be used in STDA and SRPA, but this would require the construction of c.m. spurious states in 2p-2h basis.

The EMPM is exactly identical to STDA within the space encompassing 1p-1h plus 2p-2h configuration under the simplifying assumption of neglecting the coupling between the HF and the 2p-2p basis states. However, the anomaly of the ^{48}Ca spectrum, where the 2^+ falls below the HF ground state, ratifies the failure of STDA and SRPA in describing the spectroscopy of some nuclei, at least for the potential adopted here. The EMPM shows how to remove this anomaly. One should refer the levels to a fully correlated ground state by taking into account the HF to 2p-2h coupling jointly with enlarging the configuration space so as to include the 3p-3h basis, as it was done in [35]. In other words, one should move to full shell model or to the EMPM.

The EMPM is more general than STDA and is exactly identical to shell model within a given configuration space. With respect to shell model, it is more involved but offers significant advantages. It allows for truncations of the multiphonon basis even if a large space including very high energy configurations is adopted. These are accounted for by the TDA phonons building up the n-phonon states. It is suitable for investigating low energy spectra as in shell model but also the high energy responses as in RPA or SRPA. Last, but not least, the intrinsic motion is decoupled completely and exactly from the c.m. motion for any s.p. basis and under no restrictions.

ACKNOWLEDGMENTS

This work was partly supported by the Czech Science Foundation (Czech Republic), P203-19-14048S and by the Charles University Research Center UNCE/SCI/013. The work of P.P. was supported by the Rare Isotope Science Project of the Institute for Basic Science funded by the Ministry of Science, ICT and Future Planning and the National Research Foundation (NRF) of Korea (2013M7A1A1075764). P.V. thanks the INFN for financial support. Computational resources were provided by the CESNET LM2015042 and the CERIT Scientific Cloud LM2015085, under the program "Projects of Large Research, Development, and Innovations Infrastructures". This work is co-funded by EU-FESR, PON Ricerca e Innovazione 2014-2020 - DM 1062/2021.

[1] P. Ring and P. Schuck, *The Nuclear Many-Body Problem* (Springer-Verlag, New York, 1980).
[2] M. Harakeh and A. van der Woude, *Giant Resonances* (Oxford University Press, New York, 2001).
[3] A. Bohr and B. R. Mottelson, *Nuclear Structure* (World Scientific Publishing Company, New York, 1998).
[4] V. Soloviev, *Theory of Atomic Nuclei: Quasiparticles and Phonons* (Institute of Physics Publishing, Bristol, 1992).
[5] N. Lo Iudice, C. Y. Yu Ponomarev, C. Stoyanov, A. V. Sushkov, and V. V. Voronov, J. Phys. G: Nucl. Part. Phys. **39**, 043101 (2012).
[6] G. F. Bertsch, P. F. Bortignon, and R. A. Broglia, Rev. Mod. Phys. **55**, 287 (1983).
[7] Y. F. Niu, G. Colò, and E. Vigezzi, Phys. Rev. C **90**, 054328 (2014).
[8] E. V. Litvinova and V. I. Tselyaev, Phys. Rev. C **75**, 054318 (2007).
[9] E. Litvinova, P. Ring, and V. Tselyaev, Phys. Rev. C **75**, 064308 (2007).
[10] E. Litvinova and P. Schuck, Phys. Rev. C **100**, 064320 (2019).
[11] E. Litvinova and Y. Zhang, Phys. Rev. C **104**, 044303 (2021).
[12] D. Gambacurta, M. Grasso, and J. Engel, Phys. Rev. C **92**, 034303 (2015).
[13] D. Gambacurta, M. Grasso, V. De Donno, G. Co', and F. Catara, Phys. Rev. C **86**, 021304(R) (2012).
[14] J. Wambach, Rep. Prog. Phys. **51**, 989 (1988).
[15] P. Papakonstantinou and R. Roth, Phys. Lett. B **671**, 356 (2009).

[16] P. Papakonstantinou and R. Roth, Phys. Rev. C **81**, 024317 (2010).
[17] H. Feldmeier, T. Neff, R. Roth, and J. Schnack, Nucl. Phys. A **632**, 61 (1998).
[18] V. I. Tselyaev, Phys. Rev. C **75**, 024306 (2007).
[19] V. I. Tselyaev, Phys. Rev. C **88**, 054301 (2013).
[20] F. Andreozzi, F. Knapp, N. Lo Iudice, A. Porrino, and J. Kvasil, Phys. Rev. C **75**, 044312 (2007).
[21] F. Andreozzi, F. Knapp, N. Lo Iudice, A. Porrino, and J. Kvasil, Phys. Rev. C **78**, 054308 (2008).
[22] D. Bianco, F. Knapp, N. Lo Iudice, F. Andreozzi, and A. Porrino, Phys. Rev. C **85**, 014313 (2012).
[23] G. De Gregorio, F. Knapp, N. Lo Iudice, and P. Veselý, Phys. Rev. C **93**, 044314 (2016).
[24] G. De Gregorio, F. Knapp, N. Lo Iudice, and P. Veselý, Phys. Rev. C **94**, 061301(R) (2016).
[25] G. De Gregorio, F. Knapp, N. Lo Iudice, and P. Veselý, Phys. Rev. C **95**, 034327 (2017).
[26] G. De Gregorio, F. Knapp, N. Lo Iudice, and P. Veselý, Phys. Scr. **92**, 074003 (2017).
[27] G. De Gregorio, F. Knapp, N. Lo Iudice, and P. Veselý, Phys. Rev. C **97**, 034311 (2018).
[28] G. De Gregorio, F. Knapp, N. Lo Iudice, and P. Veselý, Phys. Rev. C **99**, 014316 (2019).
[29] G. De Gregorio, F. Knapp, N. Lo Iudice, and P. Veselý, Phys. Rev. C **101**, 024308 (2020).
[30] D. J. Rowe, Rev. Mod. Phys. **40**, 153 (1968).
[31] C. Yannouleas, Phys. Rev. C **35**, 1159 (1987).
[32] P. Papakonstantinou, Phys. Rev. C **90**, 024305 (2014).
[33] V. Tselyaev, Phys. Rev. C **106**, 064327 (2022).
[34] D. Bianco, F. Knapp, N. Lo Iudice, P. Veselý, F. Andreozzi, G. De Gregorio, and A. Porrino, J. Phys. G: Nucl. Part. Phys. **41**, 025109 (2014).
[35] G. De Gregorio, F. Knapp, N. Lo Iudice, and P. Veselý, Phys. Lett. B **821**, 136636 (2021).
[36] G. De Gregorio, F. Knapp, N. Lo Iudice, and P. Veselý, Phys. Rev. C **105**, 024326 (2022).
[37] D. Gambacurta, M. Grasso, and F. Catara, J. Phys. G: Nucl. Part. Phys. **38**, 035103 (2011).
[38] D. Bianco, F. Knapp, N. Lo Iudice, F. Andreozzi, A. Porrino, and P. Vesely, Phys. Rev. C **86**, 044327 (2012).
[39] R. B. Wiringa, V. G. J. Stoks, and R. Schiavilla, Phys. Rev. C **51**, 38 (1995).
[40] G. Colò, L. Cao, N. Van Giai, and L. Capelli, Comput. Phys. Commun. **184**, 142 (2013).
[41] D. Thouless, Nucl. Phys. **22**, 78 (1961).
[42] D. Rowe, *Nuclear Collective Motion: Models and Theory* (Methuen, London, 1970).